Probing the 3-step Lithium Storage Mechanism in $CH_3NH_3PbBr_3$ Perovskite Electrode by *Operando*-XRD Analysis

Nuria Vicente[a], Dominic Bresser[b,c], Stefano Passerini[b,c] and Germà Garcia-Belmonte[a,*]

[a] Institute of Advanced Materials (INAM), Universitat Jaume I, 12006 Castelló, Spain

[b] Helmholtz Institute Ulm (HIU), Helmholtzstrasse 11, 89081 Ulm, Germany

[c] Karlsruhe Institute of Technology (KIT), P.O. Box 3640, 76021 Karlsruhe, Germany

*Corresponding author's e-mail: G. Garcia-Belmonte (garciag@uji.es)

Abstract

Organic-inorganic hybrid materials have gradually become one of the most actively studied research fields due to their fascinating properties. The reaction between lithium and organic-inorganic halide perovskite has just recently been proposed. However, the exact mechanisms taking place in this electrode material have not been fully elucidated, yet. To shed light on these processes an *operando*-X-ray diffraction study has been performed and is reported herein. According to our results the lithiation of $CH_3NH_3PbBr_3$ entails three reaction steps, distinguishable during the initial galvanostatic lithiation for different Li-ion molar contents x: (1) the initial Li^+ insertion into the perovskite phase in which pure perovskite and lithiated phases coexist ($0 < x < 1$), (2) the perovskite conversion reaction leading to the formation of metallic lead ($1 < x < 2$), and finally, (3) the alloying of lithium with the metallic lead previously formed. In more detail, for $x > 0.3$, the formation of a Li_x:$CH_3NH_3PbBr_3$ phase with distinctive X-ray diffraction peaks is clearly detected, which coexists with the pristine material, till abruptly both phases disappear at $x \sim 1$ and CH_3NH_3Br and Pb metal are formed. It is shown that this conversion reaction is an irreversible process. The proposed mechanism for lithium storage gives a complete perspective of the complex structural environment involving the use of perovskite materials as electrodes for Li-ion batteries.

TOC figure:

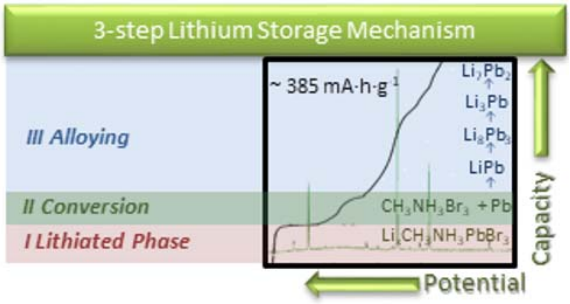

A Table of Contents text:

By *operando*-X-ray diffraction analysis, lithiation of $CH_3NH_3PbBr_3$ occurs through three reaction steps. For Li-ion molar contents ($0 < x < 1$), perovskite and lithiated phases coexist without drastic structural reordering. A conversion reaction leading to the formation of metallic lead ($1 < x < 2$) is observed, followed by the alloying of lithium with the metallic lead previously formed ($x > 2$).

1. Introduction

Studies on the already well-established Li-ion battery (LIB) technology are focusing on novel lithium storage materials and electrode architectures, enhancing the cycling stability and safety as well as lowering the overall cost through the design of innovative materials. A recent publication proposed the use of organic-inorganic hybrid perovskite materials as promising anodes to improve the battery performance of LIBs [1]. These materials attract tremendous scientific attention in the field of photovoltaics since 2009 when the first application of hybrid perovskites in solar cells was reported [2]. The revolution in the use of hybrid perovskites for solid state solar cells started in 2012, when photovoltaic power conversion efficiencies of 9.7% and 10.9%, were reported [3, 4]. Motivated, moreover, by its prominent properties (high absorption coefficient, low charge-carrier recombination rates, as well as easy and low cost of cell fabrication by chemical methods and abundance of raw materials) further work lead to the achievement of impressive power conversion efficiencies of more than 20.0% [5]. Furthermore, because of their ability to host extrinsic elements such as Li^+ or Na^+, while simultaneously exhibiting high ion diffusivity, its potential for battery applications should be deeply studied. However, a complete analysis of the mechanisms taking place during the charge and discharge processes in these kind of electrodes has not been reported, yet.

The first works exploring hybrid perovskites as storage materials and the early proposed mechanisms have been based on *ex-situ* experiments. The first report dates from 2015. Therein, methylammonium lead halide perovskites were suggested as active material for Li-ion battery anodes by Xia et al. [1]. The authors prepared $CH_3NH_3PbI_3$ and $CH_3NH_3PbBr_3$ by hydrothermal synthesis, characterized them as anodes, and demonstrated first cycle discharge capacities of 43.6 and 331.8 $mA \cdot h \cdot g^{-1}$, respectively. After 200 charge–discharge cycles, the capacity was still 121 $mA \cdot h \cdot g^{-1}$ in the case of $CH_3NH_3PbBr_3$ with a relative capacity retention of 76.9%, highlighting the important role of the composition of organometallic halide perovskite (AMX_3) on the lithium storage performance.

Afterwards, numerous groups working on perovskite materials and/or batteries have entered this research subject –either with studies on innovative hybrid materials or theoretical calculations to evaluate the electrochemical performance. The influence of composition and crystalline structure, as two important factors contributing to the high de-/lithiation capacity and reversibility, have been studied by Tathavadekar et al. [6]. They showed that the specific capacity and cycling stability can be improved by tuning the dimensionality of halide-perovskites from 3D to 1D. It is said that the molecularly engineered low-D perovskites exhibit an open structure, which adopts a morphology favorable for facile ion access. The benzidine-mediated, 1D lead iodide-based perovskites show high reversible capacity values of 646 $mA \cdot h \cdot g^{-1}$ with great cycling

stability [6]. These parameters are superior in comparison to the usual 3D lead iodide based perovskite. By performing *ex-situ* XRD, it was revealed that the storage primarily occurs *via* the Li_xPb alloying process. Meanwhile, a deeper study on the 2D hybrid perovskite using powder composite electrodes was carried out by Ramirez et al. [7]. They reported that 3D $CH_3NH_3PbBr_3$ reached a high discharge capacity of ~500 $mA{\cdot}h{\cdot}g^{-1}$, followed by a reduced charge capacity of 160 $mA{\cdot}h{\cdot}g^{-1}$. It was proposed that this irreversibility resulted also from other processes taking place during the lithiation reaction, since the newly synthesized 2D $(CH_3NH_3)_2(CH_3(CH_2)_2NH_3)_2Pb_3Br_{10}$ with a layered structure showed 100% reversibility during cycling with capacities of ~375 $mA{\cdot}h{\cdot}g^{-1}$. As a consequence, it has been concluded that 2D layered structures are advantageous for the reversible lithium-ion storage. The authors, moreover, contributed to an enhanced understanding of the lithium insertion/extraction mechanism by revealing the initial occurrence of the intercalation process in the hybrid material, accompanied by the reversible alloying process of the Li_xPb intermetallic compounds formed.

On the other hand, also the properties of lithium-doped $CsPbBr_3$ all-inorganic perovskite have been studied [8]. It has been reported in that study that lithium doping enhances the light emission of LEDs with low turn-on voltage and its absorption of light. It was further found that the lithium doping leads to a diamagnetic behavior, PL blue-shift, as well as higher photovoltage and photocurrent behavior, indicating that the presence of lithium can improve the photovoltaic performance of the material. The doping ratio, however, was controlled to avoid the degradation of the perovskite structure. Nonetheless, the electrochemical studies evidenced that about three lithium ions can be doped in the $CsPbBr_3$ crystal [9]. In a recent publication [10], the protocol for electrochemical tests of all-inorganic $CsPbBr_3$ and hybrid organic−inorganic $CH_3NH_3PbI_3$ perovskites has been proposed. By *ex-situ* experiments, such as XRD, XPS, SEM-EDX analysis, it has been shown that metallic Pb is eventually formed upon reduction [10]. During oxidation and reduction, the Br^- and Pb^{2+}, respectively, are gradually decreasing due to the degradation of the $CsPbBr_3$ structure. Two oxidation steps and one reduction step were revealed by spectroelectrochemical studies, at potentials of +0.8 V, +1.1 V, and −0.75 V vs. Ag/Ag^+, respectively. These redox processes were coupled with the decrease in the absorbance related to $CH_3NH_3PbI_3$ and its degradation rate.

The complete mechanism of the hybrid perovskite electrode operation has been proposed very recently [11]. A combination of simulation methods (density functional theory, DFT, with the *ab initio* code VASP) and *ex-situ* powder X-Ray diffraction (PXRD) techniques has been used to analyze a wide variety of electronic, structural, and defect properties of hybrid halide perovskites as Li-ion battery active material. The calculations revealed a conversion process to lithium halides (LiX) and Pb metal, which dominates the electrode reactions, particularly for $CH_3NH_3PbBr_3$ and $CH_3NH_3PbCl_3$.

In our previous publication [12], we obtained high capacity values for $CH_3NH_3PbBr_3$ upon the first discharge, i.e., ~600 $mA \cdot h \cdot g^{-1}$, followed by an important decrease in the second cycle to ~400 $mA \cdot h \cdot g^{-1}$, and finally delivering a stable capacity of ~200 $mA \cdot h \cdot g^{-1}$. This is interpreted as an indication that additional processes are taking place, such as the formation of a solid electrolyte interphase (SEI) and changes in the perovskite structure [7, 11]. The theoretical discharge capacity for these materials is close to 50 $mA \cdot g^{-1}$, for a Li-ion molar fraction of $x = 1$ in the pristine hybrid materials for an insertion mechanism. Accordingly, the processes taking place during lithiation are very complex and some kind of electrode restructuring is occurring. Moreover, by electrochemical impedance spectroscopy the diffusivity coefficient in $CH_3NH_3PbBr_3$ was determined, providing diffusivity values as high as $D_\mu \approx 10^{-7}$ cm^2 s^{-1} [13]. This value highlights the fast ionic conductivity of hybrid perovskite compounds, as recently corroborated for intrinsic defect migration [14].

Here, we elucidate the complexity of the mechanisms taking place in $CH_3NH_3PbBr_3$ when utilized as lithium-ion anode material. The structural evolution of $CH_3NH_3PbBr_3$ is studied by *operando*-XRD during the discharge–charge (lithiation-delithiation) process, revealing for the first time that the hybrid perovskite material suffers a critical crystal structure rearrangement at Li^+ molar contents higher than 1. Before this limit, the pure perovskite phase is maintained despite the high Li^+ density, coexisting with a lithiated phase and the formation of metallic Pb. For $1 < x < 2$, the presence of the CH_3NH_3Br precursor is detected, signaling the occurrence of the conversion reaction, leading to the formation of Pb^0. For a higher Li^+ molar content, $x > 2$, the alloying reaction occurs, resulting in the formation of the Li-Pb alloy. Moreover, the substantial irreversibility observed for the first cycle is associated with the conversion reaction, as also reflected by the corresponding electrochemical response.

2. Experimental

The perovskite material was synthesized by the slow solvent evaporation from a solution containing stoichiometric amounts of lead bromide ($PbBr_2$, TCI) and methylammoniumbromide (CH_3NH_3Br, >98% TCI) in *N,N*-dimethylformamide (DMF, Sigma-Aldrich), resulting in the formation of an orange precipitate. A Bruker AXS-D4 Endeavor Advance X-ray diffractometer using Cu Kα, wavelength λ = 1.5406 Å, is employed for the X-ray diffraction (XRD) analysis to confirm the phase-pure perovskite crystallographic structure [12].

Perovskite-based electrodes were prepared by casting slurries, which solid content was 80 wt% active material ($CH_3NH_3PbBr_3$; 65 nm average size particles), 10 wt% Super C65 (TIMCAL), and 10 wt% PVdF (5130 Solvay), dispersed in *N*-methyl-2-pyrrolidone as solvent, on copper foil (Schlenk). Li metal foil (battery grade, Honjo

Metal Co.) was used as the counter and reference electrode and an electrolyte-soaked sheet of glass fiber (Whatman) was employed as separator. The electrolyte was 1M lithium hexafluorophosphate ($LiPF_6$, Sigma-Aldrich) in ethylene carbonate, ethyl-methyl carbonate, and dimethyl carbonate (EC:EMC:DMC = 1:1:1 vol; UBE). Cell assembly was carried out in an argon-filled glovebox with O_2 and H_2O content lower than 1 ppm.

The study of the Li uptake mechanism was performed via *operando*-XRD analysis coupled with galvanostatic lithiation (discharge) and delithiation (charge) steps. The *operando*-XRD study was performed using the Cu K_α radiation on the D8 Advance (Bruker) in Bragg–Brentano mode. Electrodes were prepared by casting the active material slurry directly on the beryllium (Be) window, which served as current collector and "window" for the X-ray beam.[15] The active material mass loading of the electrodes was about 10 $mg \cdot cm^{-2}$. The assembled cell was allowed to rest for one hour. Subsequently, the cell was galvanostatically cycled by means of a Solartron 1287 potentiostat, applying a specific current of 10 $mA \cdot g^{-1}$, calculated according to a complete discharge (cathodic cut-off potential: 0.05 V) in 37.8 h. In parallel, XRD analysis was performed within a 2θ range of 10° to 50° and with a step size of 0.02°, resulting in a complete scan every 30 min. After discharging to 0.05 V, the cell was charged to an anodic cut-off potential of 1.80 V. All potential values reported in this work refer to the Li/Li^+ quasi-reference couple and all capacity data are normalized to the mass of the $CH_3NH_3PbBr_3$ active material. Further details regarding the structural, morphological, and electrochemical characterization of the active material can be found in our previous works [12, 13].

3. Results and discussion

$CH_3NH_3PbBr_3$ is gaining interest as a negative electrode material for Li-ion batteries because of its high specific capacity exceeding the specific capacity of graphite and $Li_4Ti_5O_{12}$ [16]. However, the various intermediate conversion and alloying reactions occurring during lithiation/delithiation, as well as the electrolyte stability have not been fully elucidated and many ambiguities remain. In **Figure 1a,** the galvanostatic charge-discharge curves of the perovskite-based electrode at a specific current of 100 $mA \cdot g^{-1}$ are shown and several voltage plateaus are observed. During the first discharge, a first plateau is observed at around 2.3 V vs. Li/Li^+, where Li is assumed to be inserted into the perovskite structure. Between 2.3 and 1.85 V vs. Li/Li^+, it is assumed that $CH_3NH_3PbBr_3$ and $Li_xCH_3NH_3PbBr_3$ phases coexist. The subsequent plateau at 1.4 V is presumably related to the formation of Pb^0 through the conversion reaction. Then, between 0.60 and 0.29 V vs. Li/Li^+, several Li_xPb_y phases with increasing lithium content are formed. The first discharge will be explained in more detail below. Following the first discharge process, a significant irreversibility is observed. The

material is unable to recover the initial capacity, which dramatically fades during the initial 10 cycles. In fact, no XRD signal corresponding to $CH_3NH_3PbBr_3$ can be observed even after the complete galvanostatic delithiation (Figure 1b), indicating that the initial conversion reaction is essentially irreversible and only the subsequent alloying process provides the observed charge-discharge capacities.

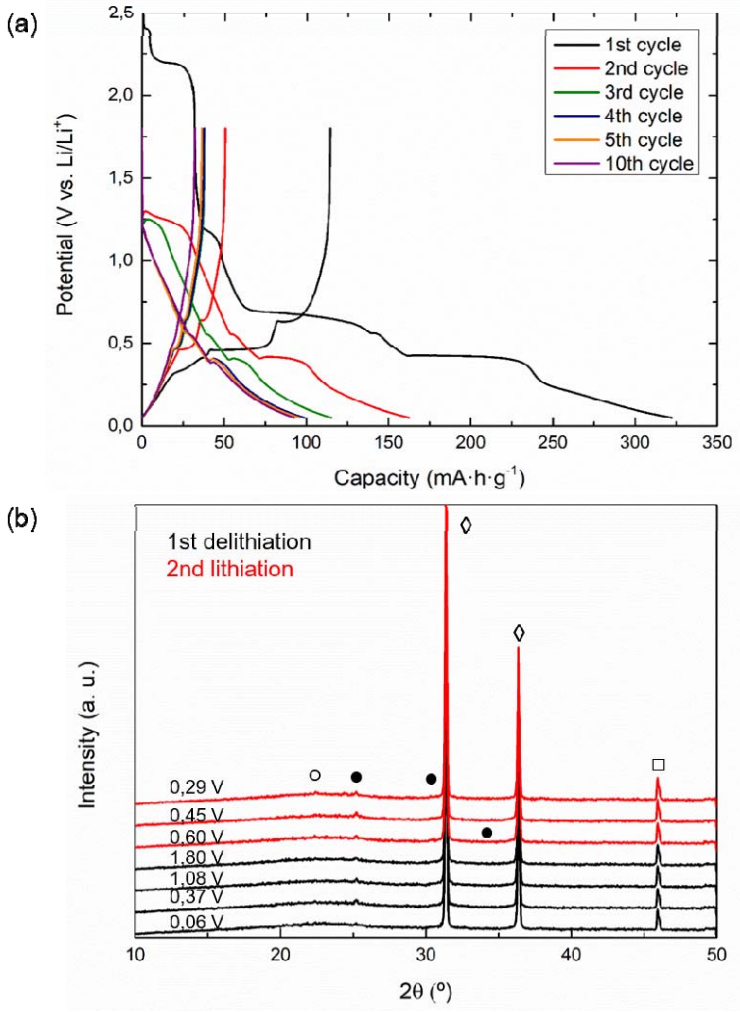

Figure 1. (a) Galvanostatic dis-/charge profiles for $CH_3NH_3PbBr_3$ as lithium-ion active material at a specific current of 100 $mA \cdot g^{-1}$ for the first 10 cycles. (b) In *operando*-XRD scans corresponding to the alloying stage during the first delithiation and second lithiation: (○) Li_8Pb_3,(•) LiPb, (◊) Pb and (□) Be.

The *operando*-XRD patterns obtained during the first lithiation of the sample (galvanostatic discharge down to 0.05 V) are presented in **Figure 2**. The diffractograms show that $CH_3NH_3PbBr_3$ is always present at potentials higher than 1.85 V. For the pristine material (red diffractograms in Figure 2), the characteristic perovskite reflections are observed, whose corresponding lattice parameter (a = 5.9394 Å; space group: P3-m3) is in good agreement with a previous report [1]. For the first stage of the discharge curve, a reflection at 45.9º is observed, which corresponds to the overlapping

of two reflections related to the perovskite and metallic beryllium. After the conversion stage, only the beryllium reflection is observed (space group $P6_3/mmc$, $a = b = 2.285$ Å and $c = 3.622$ Å).

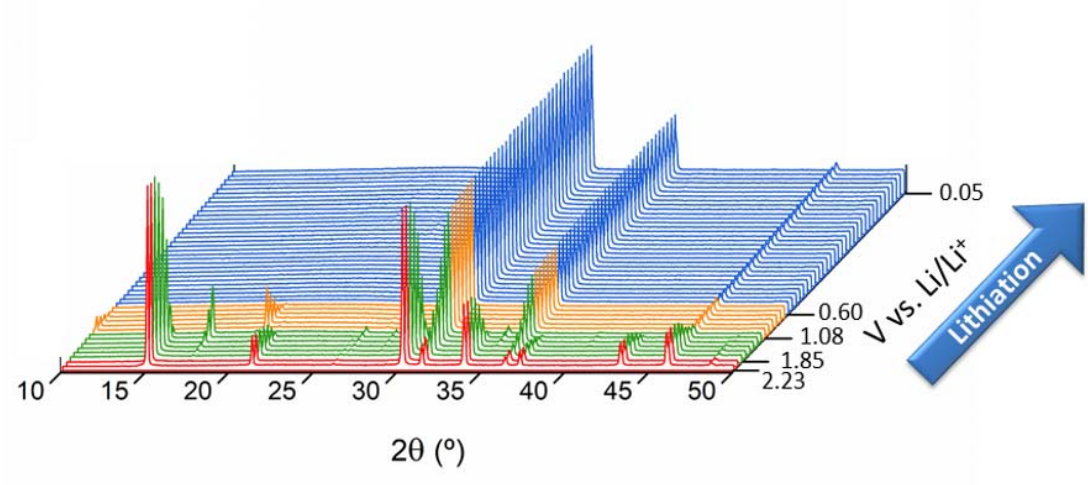

Figure 2. First discharge *operando*-XRD patterns recorded for the $CH_3NH_3PbBr_3$–based electrode. Different stages are indicated by different colors: Stage I: pristine material (red) and lithiated phase (green); Stage II: conversion (orange); and Stage III: alloying (blue).

The *operando*-XRD measurement reveals that the pristine perovskite active material is detected only at the beginning, i.e., for the four first XRD patterns (red diffractograms in Figure 2). A new phase is formed, when the Li^+ molar content approaches $x \sim 0.3$. The appearance of diffraction peaks at 17.3º, 26.5º, 28.3º, 33.3º, 35.0º, and 40.5º can be attributed to the formation of a lithiated phase Li_x:$CH_3NH_3PbBr_3$ that distorts the perovskite structure (green diffractograms in Figure 2). Therefore, two phases coexist for a Li^+ molar content of $x < 1.08$ (stage I). In addition, the appearance and growth of two reflections at 31.2º and 36.3º, corresponding to metallic Pb, are observed, presumably indicating the concurrence of the conversion reaction at least on the active material particles surface. During this stage (green XRD patterns in Figure 2), the characteristic perovskite diffraction peaks become weaker upon further lithiation, while the reflections for the lithiated phase become more evident. Both phases (pure $CH_3NH_3PbBr_3$ and lithiated Li_x:$CH_3NH_3PbBr_3$) disappear abruptly at the beginning of the next stage, which occurs for a lithium content of $x > 1.08$ and a cell voltage of 1.85 V vs. Li/Li^+ (stage II; orange diffractograms). It appears that the structure cannot insert more Li^+ without severe structural distortions and, as a consequence, the cubic structure vanishes. **Figure 3** shows the proposed transformation diagram, which links the characteristic XRD patterns for each stage with the discharge profile, specific capacity, and lithium content.

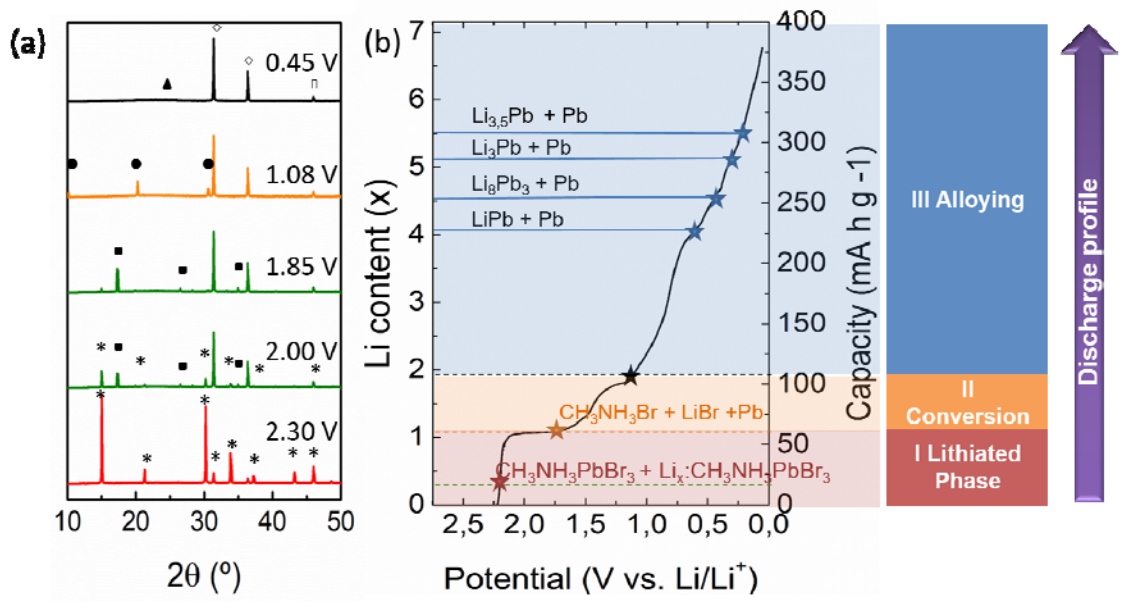

Figure 3. (a) Selected characteristic *operando*-XRD patterns of $CH_3NH_3PbBr_3$ for every stage: (*) $CH_3NH_3PbBr_3$, (▪) $Li_xCH_3NH_3PbBr_3$, (•) CH_3NH_3Br, (▲) Li_8Pb_3 (better resolution Fig. 1.b), (◊) Pb, and (□) Be. (b) The recorded discharge profile, where each stage is highlighted in a different color: First, the pure material (red), and lithiated phase (red); second, the conversion stage (orange), and, third, the alloying stage (blue). The occurring alloying reactions, i.e., the different lithium/lead phased are provided in the figure.

When the pristine material and the lithiated phase disappear, new diffraction peaks are observed at 10.1º and 20.3º, as shown in Figure 3a. The new diffraction peaks correspond to the CH_3NH_3Br precursor [17], indicating the loss of the initial perovskite structure and the occurrence of a conversion reaction according to $Li{:}CH_3NH_3PbBr_3 \rightarrow CH_3NH_3Br + LiBr + Pb$ (stage II). This phase, however, disappears at the end of the conversion stage, i.e., for a Li^+ molar content of $x \sim 2$, it could be caused by its dissolution in electrolyte, such is actually the case for LiBr. In agreement with previous XRD results,[18] the plateau in the discharge profile near ~1.08 V vs. Li/Li^+ corresponds to the Pb(II) → Pb(0) reduction process. It is possible to identify two reflections at 31.2º and 36.3º, which can be matched to metallic Pb (space group Fm3m, a = 4.951 Å).

Subsequently, the Li-Pb alloying starts ($x > 2$; stage III). The corresponding plateaus in the discharge profile between 0.4−0.6 V vs. Li/Li^+ are associated with the formation of different Li-Pb phases, such as LiPb, Li_8Pb_3, Li_3Pb, and $Li_{3.5}Pb$, which have been also identified in the same voltage range for electrodes based on pure lead metal.[18] For our *operando*-XRD, first, one new, relatively weak reflection appears at 25.29º, which is assigned to the formation of LiPb (see also Figure 1b). After $x \sim 4.1$, this reflection

disappears and another new diffraction peak is observed at 22.3º, corresponding to Li_8Pb_3. The occurrence of these two phase transitions are related to the two voltage plateaus at 0.601 V and 0.449 V, respectively. Finally, the formation of Li_3Pb is observed ($2\theta \sim 23º$), while no appreciable reflection for the formation of $Li_{3.5}Pb$ is detected. At the end of the discharge process, around 6 Li^+ per formula unit of the perovskite has been stored in the electrode. After all, the reverse evolutions of diffraction peaks corresponding to Pb and Li-Pb alloys can be followed down to 1.5 V vs. Li/Li^+ (Figure 1b) [18]. The irreversibility of the conversion reactions leave the alloying reaction as the only storage mechanism, as also confirmed by the long-term cycling experiments and in accordance with previous studies [1, 7, 12].

Based on this *operando*-XRD analysis, we propose the following series of electrochemical reactions for the complete lithiation mechanism, shown in **Table 1**. In Figure 3b the lithiated phase and conversion products as well as the alloying reactions are shown, accompanying the discharge curve and the potentials of the observed plateaus. Based on these reactions, the theoretical discharge capacity of the investigated perovskite material (for $x \sim 6$) is around 358 $mA{\cdot}h{\cdot}g^{-1}$. By calculating the potential derivative of the initial lithiation curve as $-dQ/dV$, one can observe a set of reaction peaks (Supporting Information) that corroborate the proposed mechanisms.

Table 1. Lithium content, products formed at characteristics potentials, and the electrode's capacity for the different stages: lithiated phase, conversion, and alloying.

Li^+ content x	**Detected Phases**	**End Potential of Stage (V vs. Li/Li^+)**	**Capacity ($mA{\cdot}h{\cdot}g^{-1}$)**	**Stage**
$0.00 < x < 1.10$	$CH_3NH_3PbBr_3$ $Li_xCH_3NH_3PbBr_3$	≈ 1.85	≈ 55	I Lithiated Phase
$1.10 < x < 1.90$	CH_3NH_3Br LiBr Pb	≈ 1.08	≈ 110	II Conversion
$1.90 < x < 4.10$	Pb	≈ 0.60	≈ 225	III Alloying
$4.10 < x < 4.50$	Pb LiPb	≈ 0.60	≈ 225	
$4.50 < x < 5.15$	Pb Li_8Pb_3	≈ 0.45	≈ 255	
$5.15 < x < 5.50$	Pb Li_3Pb	≈ 0.37	≈ 285	
$x > 5.50$	Pb $Li_{3.5}Pb$	≈ 0.29	≈ 315	

The proposed mechanism comprises the occurrence of different stages: First, an insertion mechanism, for which only the initial perovskite structure is present (stage I),

followed by further lithiation until the appearance of the lithiated phase; the second stage is characterized by a pure conversion reaction (stage II), before eventually reaching the final alloying stage III. The stages I and II are irreversible, causing the greatly modified electrochemical response after the first full lithiation. On the other hand, the alloying reactions are considered to be partially reversible reactions as it is evidenced in Figure 1a. Lead alloying reaction reversibility was deeply studied in previous work [19].

4. Conclusions

In summary, this exhaustive experimental study reports *operando*-XRD results for an organic-inorganic halide perovskite-like anode for Li-ion batteries, $CH_3NH_3PbBr_3$. It has been probed that the lithiation proceeds by a complex 3-step storage mechanism in this electrode material. Li-ion insertion is followed by conversion processes with the eventual formation of CH_3NH_3Br and metallic Pb. After these stages, the metallic lead is alloying with lithium by forming a series of Li-Pb phases: LiPb, Li_8Pb_3, and Li_3Pb. The findings reveal that the structural evolution of such organic-inorganic perovskite during the first lithiation process is largely irreversible, which explains the extensive capacity fading after the first discharge. This work proposes a complete mechanism for perovskite-based electrodes with important insights that are anticipated to foster their potential application in the field of batteries. Moreover, these insights into the reaction mechanism and ion accommodation into the crystal structure may guide also the application of lithium-doped perovskites in the field of solar cells, as Li-containing solar cells show a varying hysteresis depending on the scan rate due to the different kinetics of extrinsic and intrinsic ion migration [20].

Author Information.

Corresponding author: garciag@uji.es

ORCID

Nuria Vicente: 0000-0002-9823-7131

Dr. Dominic Bresser: 0000-0001-6429-6048

Prof. Stefano Passerini: 0000-0002-6606-5304

Prof. Germà Garcia-Belmonte: 0000-0002-0172-6175

Notes

The authors declare no competing financial interest.

Acknowledgments

We are grateful for financial support by Ministerio de Economía y Competitividad (MINECO) of Spain under Project (MAT2016-76892-C3-1-R). N. Vicente acknowledges Universitat Jaume I (UJI) through FPI Fellowship Program (PREDOC / 2015/54) and (E-2017-18) within framework of Action 2 of the Mobility Program for Research Staff under the 2017 Research Promotion Plan. SCIC from Universitat Jaume I is also acknowledged.

Keywords

Extrinsic ion, hybrid perovskite, lithium doping, storage mechanism, X-ray diffraction

References

[1] H.-R. Xia, W.-T. Sun, L.-M. Peng *Chem. Commun*. **2015**, *51*, 13787-13790.

[2] A. Kojima, K. Teshima, Y. Shirai, T. Miyasaka *J. Am. Chem. Soc.* **2009**, *131*, 6050-6051.

[3] L. Etgar, P. Gao, Z. Xue, Q. Peng, A. K. Chandiran, B. Liu, M. K. Nazeeruddin, M. Grätzel *J. Am. Chem. Soc.* **2012**, *134*, 17396-17399.

[4] M. Lee, J. Teuscher, T. Miyasaka, T. Murakami, H. Snaith *Science*. **2012**, *338*, 643-647.

[5] M. A. Green, Y. Hishikawa, E. D. Dunlop, D. H. Levi, J. Hohl-Ebinger, A. W. Y. Ho-Baillie *Prog. Photovoltaics Res. Appl* . **2018**, *26*, 3-12.

[6] M. Tathavadekar, S. Krishnamurthy, A. Banerjee, S. Nagane, Y. Gawli, A. Suryawanshi, S. Bhat, D. Puthusseri, A. D. Mohite, S. Ogale *J. Mater. Chem. A*. **2017**, *5*, 18634-18642.

[7] D. Ramirez, Y. Suto, N. C. Rosero-Navarro, A. Miura, K. Tadanaga, F. Jaramillo *Inorg. Chem*. **2018**, *57*, 4181-4188.

[8] Q. Jiang, X. Zeng, N. Wang, Z. Xiao, Z. Guo, J. Lu *ACS Energy Lett*. **2018**, *3*, 264-269.

[9] Q. Jiang, M. Chen, J. Li, M. Wang, X. Zeng, T. Besara, J. Lu, Y. Xin, X. Shan, B. Pan, C. Wang, S. Lin, T. Siegrist, Q. Xiao, Z. Yu *ACS Nano*. **2017**, *11*, 1073-1079.

[10] G. F. Samu, R. A. Scheidt, P. V. Kamat, C. Janáky *Chem. Mater*. **2018**, *30*, 561-569.

[11] J. A. Dawson, A. J. Naylor, C. Eames, M. Roberts, W. Zhang, H. J. Snaith, P. G. Bruce, M. S. Islam *ACS Energy Lett*. **2017**, *2*, 1818-1824.

[12] N. Vicente, G. Garcia-Belmonte *J. Phys. Chem. Lett*. **2017**, *8*, 1371-1374.

[13] N. Vicente, G. Garcia-Belmonte *Adv. Energy Mater*. **2017**, *7*, 1700710.

[14] W. Peng, C. Aranda, O. M. Bakr, G. Garcia-Belmonte, J. Bisquert, A. Guerrero *ACS Energy Lett*. **2018**, 1477-1481.

[15] D. Bresser, E. Paillard, R. Kloepsch, S. Krueger, M. Fiedler, R. Schmitz, D. Baither, M. Winter, S. Passerini *Adv. Energy Mater*. **2013**, *3*, 513-523.

[16] N. Nitta, F. Wu, J. T. Lee, G. Yushin *Mater. Today*. **2015**, *18*, 252-264.

[17] E. J. Gabe *Acta Crystallogr.* **1961**, *14*, 1296.

[18] S. M. Wood, C. H. Pham, A. Heller, C. B. Mullins *J. Electrochem. Soc*. **2016**, *163*, A1027-A1029.

[19] M. Martos, J. Morales, L. Sanchez *Electrochim. Acta*. **2003**, *48*, 615-621.

[20] Z. Li, C. Xiao, Y. Yang, S. P. Harvey, D. H. Kim, J. A. Christians, M. Yang, P. Schulz, S. U. Nanayakkara, C.-S. Jiang *Energy Environ. Sci*. **2017**, *10*, 1234-1242.